Nuclear Inst. and Methods in Physics Research, A 874 (2017) 103–112

Contents lists available at ScienceDirect

Nuclear Inst. and Methods in Physics Research, A

journal homepage: www.elsevier.com/locate/nima

VECC array for Nuclear fast Timing and angUlar corRElation studies (VENTURE)

S.S. Alam [a,b], T. Bhattacharjee [a,b,*], D. Banerjee [c], A. Saha [a,b], Deepak Pandit [a], D. Mondal [a,b], S. Mukhopadhyay [a,b], Surajit Pal [a], P. Bhaskar [a], S.K. Das [b,c,1], S.R. Banerjee [a,b]

[a] Variable Energy Cyclotron Centre, Kolkata, PIN - 700 064, India
[b] Homi Bhabha National Institute, Mumbai, PIN - 400 094, India
[c] RCD-BARC, Variable Energy Cyclotron Centre, Kolkata, PIN - 700 064, India

ARTICLE INFO

Keywords:
$CeBr_3$ scintillator detector
γ radiation
Fast timing measurement
Angular correlation coefficient
GEANT3 simulation

ABSTRACT

The VECC array for Nuclear fast Timing and angUlar corRElation studies (VENTURE) has been developed using several fast Cerium-Bromide ($CeBr_3$) scintillators coupled to Hamamatsu R9779 Photomultiplier tubes. The $CeBr_3$ detector has been characterised for the spectroscopic properties like energy response, energy resolution, timing resolution and detection efficiency. The response and efficiency of the detector have been compared with the results obtained from a Monte Carlo simulation with GEANT3 package. A time resolution of 144(1) ps and 109(1) ps was obtained for a single detector using 622–512 keV and 1173–1332 keV cascades respectively. The Generalised Centroid Difference (GCD) method has been employed with $CeBr_3$ detectors by measuring the level lifetimes for the 511.9 keV level of ^{106}Pd and the 160.6 and 383.8 keV levels of ^{133}Cs. The angular correlation measurement was performed for the 1173–1332 keV cascade in ^{60}Ni and the 228–49 keV cascade of ^{132}I nucleus, populated from the decay of ^{132}Te produced via ^{238}U(α, f) reaction.

1. Introduction

The measurement of nuclear level lifetime and transition moments carries an utmost importance in understanding the structure of the atomic nucleus, as they provide a direct access to the transition rates associated with the de-population of the nuclear levels. The timing measurement techniques have been explored in different ranges from nanosecond (ns) to picosecond (ps) [1–4], which are appropriate for in-beam prompt spectroscopy or off-beam decay spectroscopy. The measurement involves different types of γ detectors, viz., high resolution Ge as well as fast timing BaF_2. With the availability of some scintillation detectors viz., $LaBr_3$(Ce) in recent times, having energy resolution much better than the BaF_2 detectors along with a comparable time resolution, the exploration and application of an improved fast timing technique in ps range could be found in several literatures [5–9]. Recently, $CeBr_3$ scintillator detectors, which are also highly hygroscopic as $LaBr_3$, have been reported to have slightly poorer energy resolution compared to $LaBr_3$(Ce) [10] but a similar time resolution [11,12]. These detectors are being explored as viable alternative to $LaBr_3$(Ce) detectors which are limited by their self-activity [10,13] and higher price.

The measurement of energy response, energy resolution, time resolution and the efficiency of the $CeBr_3$ detectors of various sizes and coupled to different types of photomultiplier tubes (PMT) is found in several literatures [10–12,14,15]. The efficiency measurement for an $1'' \times 1''$ $CeBr_3$ detector were performed by comparing with the known efficiency of a $LaCl_3$ detector by the authors of Ref. [10]. However, the measurement of absolute detection efficiency for these detectors is absent till date to the best of our knowledge. This can be achieved by performing the measurement of detection efficiency by using a source of known disintegration per seconds (dps). The non proportionality in response of a scintillator is found below 100 keV which is the intrinsic characteristics of all scintillators [16]. The effect of this non-proportionality was found to contribute to the energy resolution of the $CeBr_3$ detectors by ~2.8% [17,18]. Also, as the high voltage in the PMT is increased to obtain better time resolution of the detector, the non-linearity in the overall energy response of the detector is found in the PMT and/or amplifier outputs. This is basically related to the saturation effect of a particular PMT and its voltage divider circuit when coupled to a fast scintillator like $LaBr_3$ or $CeBr_3$ having fast and bright scintillation

* Corresponding author at: Variable Energy Cyclotron Centre, Kolkata, PIN - 700 064, India.
E-mail address: btumpa@vecc.gov.in (T. Bhattacharjee).
[1] Retired.

http://dx.doi.org/10.1016/j.nima.2017.08.037
Received 9 May 2017; Received in revised form 11 August 2017; Accepted 21 August 2017
Available online 6 September 2017
0168-9002/

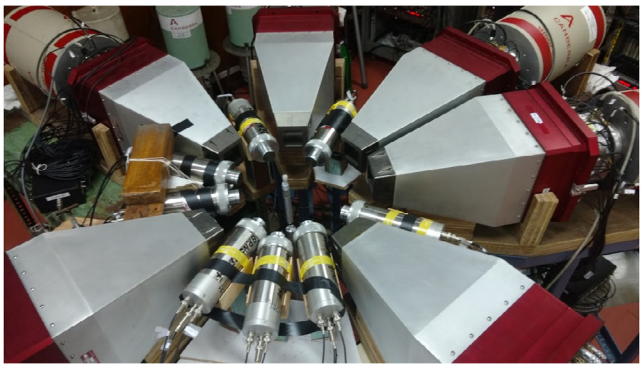

Fig. 1. (Colour online) The VENTURE array of eight $CeBr_3$ detectors coupled to the VENUS array of six clover HPGe detectors is shown.

process [19,20]. Hence, it is also important to explore the effect of the applied bias voltage of the PMT on the energy response and energy resolution of the $CeBr_3$ detectors along with their time resolution.

In the present work, the characterisation of an $1'' \times 1''$ $CeBr_3$ detector, coupled to Hamamatsu R9779 Photomultiplier tube, has been performed by measuring its energy response, energy resolution, time resolution and detection efficiency for the γ rays in a range of 80 keV to 1.4 MeV. The efficiency of one such $CeBr_3$ detector has been compared to that of a Clover HPGe detector and corroborated with a Monte Carlo simulation using GEANT3 package. Following the basic characterisation of the $CeBr_3$ detectors, an array consisting of such multiple $CeBr_3$ detectors has been set up at Variable Energy Cyclotron Centre (VECC), Kolkata. This array has been named as VECC array for Nuclear fast Timing and angUlar corRElation studies (VENTURE) and could be used in its stand alone mode as well as with the array of Clover HPGe detectors like VENUS [21] or INGA [22] for complete γ spectroscopic measurement. The array will be used for the measurement of nuclear level lifetime down to few ps and the Perturbed $\gamma - \gamma$ Angular Correlation (PAC) [23,24]. The present work reports the exploration of the Generalised Centroid Difference (GCD) method [6] (based on the Mirror Symmetric Centroid Difference (MSCD) method [5]) with the $\gamma - \gamma$ time-difference spectra, for the first time with $CeBr_3$ detectors. In addition to the lifetime measurement, the angular correlation measurement has been performed for the 1173–1332 keV and 228–49 keV cascades of ^{60}Co and ^{132}I respectively with a setup of three such $CeBr_3$ detectors on an angular correlation table, designed and fabricated at VECC, Kolkata.

2. Experimental setup

The experiment was carried out in three different configurations for the $CeBr_3$ detectors. In all the three configurations, the standard NIM based coincidence electronics and VME based data acquisition system (consisting of Mesytec MADC-32 and LAMPS data acquisition system [25]) was used. All the subsequent data analyses were done with the software program LAMPS.

In the first configuration, consisting of one $CeBr_3$ detector, the measurements of energy response, energy resolution and detection efficiency were performed. For the measurement of efficiency, the source to detector distance was kept at 16 cm.

The second configuration consists of two $CeBr_3$ detectors kept at 150°. This setup was used to measure the time resolution (cf. Section 3.3) and the $\gamma - \gamma$ time-walk characteristics using the MSCD method (cf. Section 4.2). As an extension of the second configuration, the VENTURE array was set up with eight such $CeBr_3$ detectors, as shown in Fig. 1, to explore the possibility of lifetime measurement using GCD method (cf. Section 4.3). In both these measurements, the ORTEC 584 Constant Fraction Discriminator (CFD) modules were used to generate the time pulses in Constant Fraction (CF) mode and with the use of CF delay, as and when required. In case of MSCD measurement with two detectors, one of the two CFD pulses was used as start and the other as stop respectively and fed to a Time to Amplitude Converter (TAC) module. The .AND. of these two signals were used as the trigger for acquiring data. In case of the VENTURE array, the signal processing was done by following a common start timing technique as described in Fig. 2. This is different from the timing electronics used in the previous works where centroid difference measurements have been done by using $LaBr_3$ detectors [6,26,27] and from those where GCD technique has been proposed and explored [6,27]. Hence, the present work also reports, for the first time, the use of common start timing electronics in combination with the GCD method. This method, however, requires more numbers of TAC modules compared to the method adopted in Ref. [27]. In the present work, a MASTER logic signal with $M_\gamma \geq 2$ was generated by using a majority logic unit and the width and delay matched timing outputs of the individual $CeBr_3$ detectors. This was used as the trigger to ADC and fed to the start of the TACs corresponding to all the detectors of the array. The CFD signals, appropriately delayed from start, was

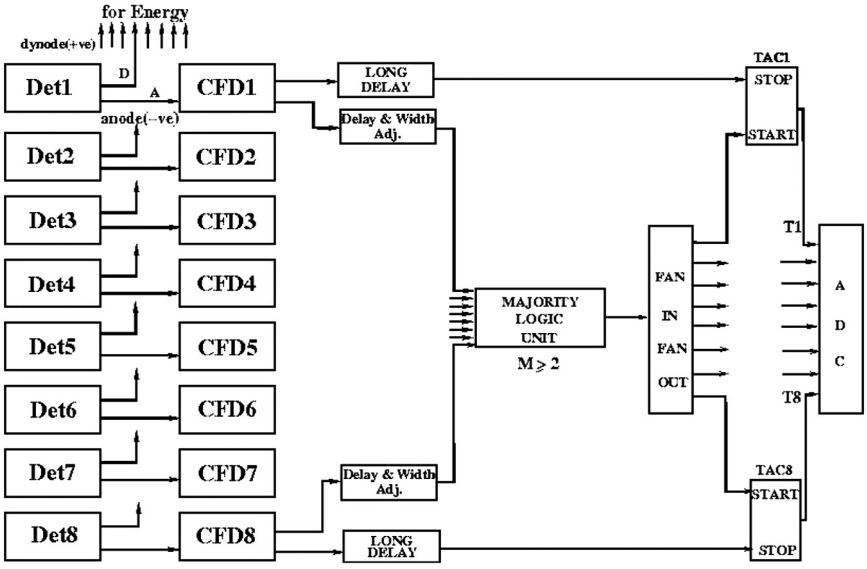

Fig. 2. The timing electronics setup used for the signal processing with the VENTURE array.

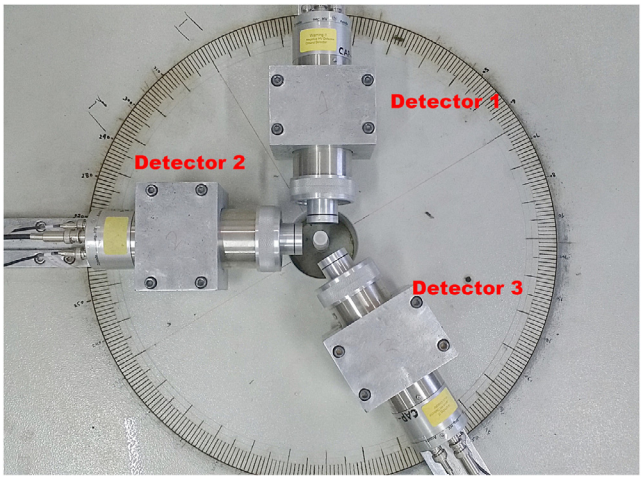

Fig. 3. (Colour online) The angular correlation setup showing three $CeBr_3$ detectors placed in closed configuration.

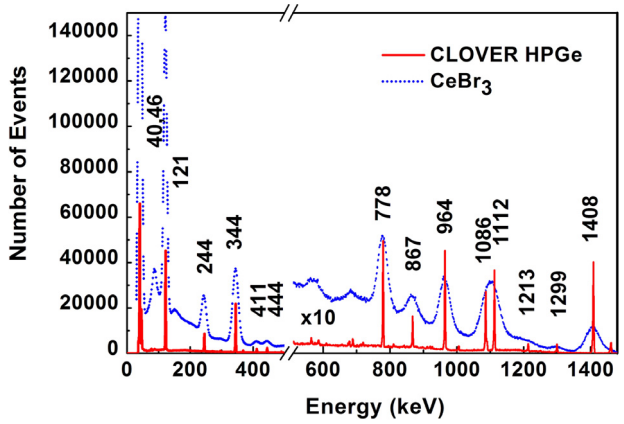

Fig. 4. (Colour online) The energy spectra obtained with $CeBr_3$ detector and Clover HPGe detector using a ^{152}Eu source.

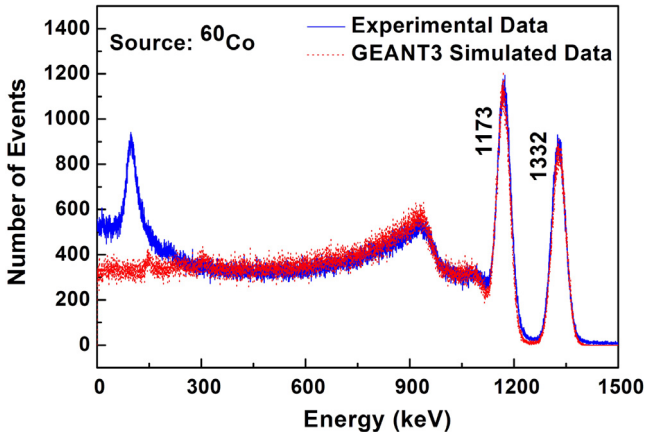

Fig. 5. (Colour online) The experimental and simulated gamma spectra for the $CeBr_3$ detector using ^{60}Co source.

given to stop of the individual TACs used in the VENTURE electronics. The coincidence data was gathered for the TAC signals corresponding to all the detectors along with their energy signals. Hence, each of these TACs (say, TAC_i) measured the time difference between the detector i and the MASTER trigger generated from the two detector hit (say $i\&j$). In the same event TAC_j will also have data that corresponds to the time difference between the detector j and the MASTER trigger. During analysis, all the energy and time parameters were gain matched to correct for the drifts observed as a function of time. The details of data sorting and the method of generating the total $\gamma-\gamma$ time difference spectra (TDS) has been discussed in Section 4.3.

In the last configuration, three detectors were placed on an angular correlation table, as shown in Fig. 3, for the measurement of $\gamma-\gamma$ angular correlation. In this configuration, the detector 1 and 2 are kept fixed and detector 3 can be moved at different angular positions with respect to Detector 1 or 2.

3. Characterisation of $CeBr_3$ detector

3.1. Energy response, resolution and linearity

The energy spectrum obtained with a $CeBr_3$ detector is shown in Fig. 4 and compared with that for a Clover HPGe detector. In Fig. 5, the experimental γ energy spectrum for a $CeBr_3$ detector obtained with a ^{60}Co source has been compared with that generated by a Monte Carlo simulation with GEANT3 package [28]. In the simulation, the different possible interaction processes of γ rays along with the exact geometrical condition of the $CeBr_3$ crystal including its window material were considered for reconstructing the γ energy spectrum. The experimental spectrum is found to be well reproduced by the simulation except the deviation observed at low energy region. This deviation could be attributed to the inherent background and the backscattered peak. However, it has been found from the existing literature that the detection of low-energy 'scattered' γ-rays (e.g., the backscatter peak) is mainly responsible for the higher background level compared to the net Compton background level [29].

The energy response of the $CeBr_3$ detectors was measured at different bias voltages of the PMT using the dynode signal while directly coupling it with a spectroscopy amplifier. The energy response was also measured by coupling the dynode output with the amplifier by introducing a preamplifier in between for all the bias voltages from −1000 to −1700V at an interval of 100V. The representative results have been displayed in Fig. 6 and it is observed that the energy response becomes non-linear after a bias voltage of −1100 V while using the direct dynode pulse. However, the response seems to become linear with the use of the preamplifier at all the bias voltages. The nonlinear response may come from the saturation effect of the PMT originated due to the bright scintillation light of $CeBr_3$ detectors [19,20]. As the biasing of the PMT was provided with a simple voltage divider circuit (VDC), the PMT appears to be entering into increased current amplification/saturation region(s) due to the high light intensity. The value of the decoupling capacitor connected at the dynode stage may not be sufficient to maintain the linearity when spectroscopy amplifier was connected directly. Nonetheless, it appears that the additional capacitor connected at the input stage of the preamplifier modifies the value of the decoupling capacitor at the last dynode stage of the PMT and thus maintaining a linear response for the entire range of the anode current.

The energy resolution of the detectors has been measured as a function of bias voltage of the PMT while using the preamplifier and shown in Fig. 7(a) for the 622 keV transition. A similar measurement has also been performed at different energy values for a fixed bias of −1200 V and is shown in Fig. 7(b). It is observed that the energy resolution of the detector remains almost constant with different bias voltages. The observed improvement in the energy resolution compared to that obtained earlier [11] is possibly because of the effect of the linearity in the response function as suggested in several studies [17,18].

3.2. Absolute efficiency

The efficiency measurement of a single $CeBr_3$ detector has been performed by using standard point sources, viz., ^{152}Eu, ^{133}Ba and ^{60}Co,

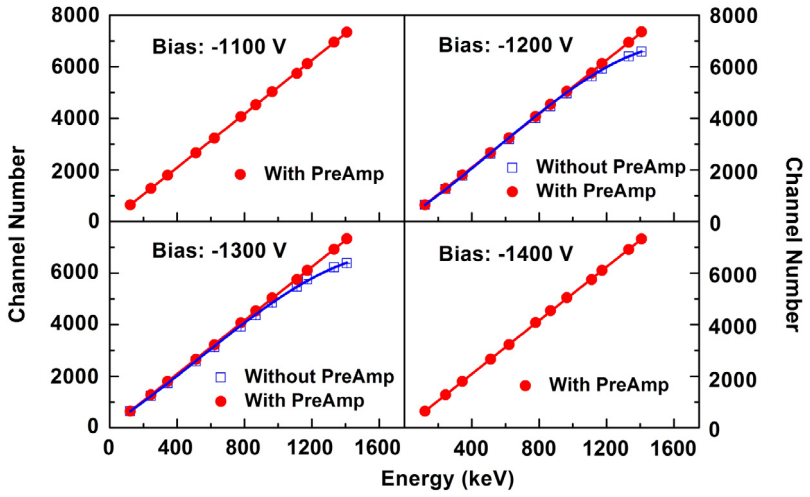

Fig. 6. (Colour online) Few representative energy response curves at different bias voltages.

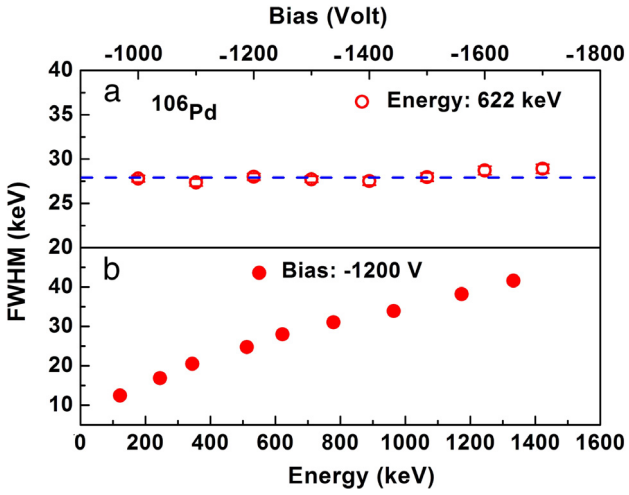

Fig. 7. (Colour online) (a) Variation of FWHM obtained at 622 keV is shown with the applied bias voltages. (b) Variation of FWHM with γ energy at a fixed bias voltage.

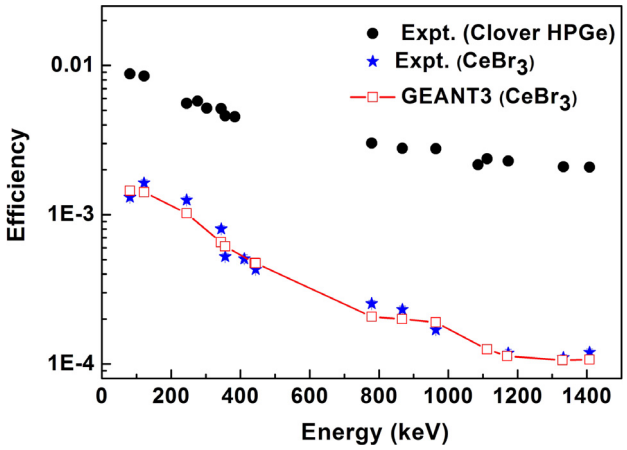

Fig. 8. (Colour online) The measured efficiency of the $CeBr_3$ detector at 16 cm is compared with GEANT3 simulation and add-back efficiency of a Clover HPGe detector.

of known disintegration per second (dps) which were kept at a distance of 16 cm from the detector. The absolute detection efficiency, which depends both on the intrinsic efficiency of the detector and the solid angle (geometric efficiency), has been extracted by using the standard formulation:

$$\epsilon_{abs} = \epsilon_{intr} \times \frac{\Omega}{4\Pi} = cps/(dps \times I).$$

Experimentally, the cps can be determined as the area under a full energy peak per unit time. I is the abundances for the particular γ transitions and were taken from ENSDF databases for the decay of the used sources [30–32]. The obtained efficiency has been plotted as a function of γ energy in Fig. 8. In the same plot, the absolute efficiency of the $CeBr_3$ detector determined from a Monte Carlo simulation with GEANT3 simulation package [28] and the efficiency of a Clover HPGe detector have also been shown. The simulation was performed as described in Section 3.1 and the result is found to be in good agreement with the experimental data. The efficiency of a Clover HPGe detector was obtained by using the add-back technique as described in Ref. [33]. It is found that the efficiency of the $1'' \times 1''$ $CeBr_3$ detector comes about 5% of the efficiency of a Clover HPGe detector at ~1 MeV.

3.3. Time resolution

The timing measurement has been performed with two $CeBr_3$ detectors at different bias voltages and with different CF delay. In order to determine the time resolution, energy gated time peaks were generated by using a Time to Amplitude Converter, as described in Section 2. A range of 50 ns was used in the TAC and the total time spectrum was displayed on a 8K spectrum. In the present work, the time resolution for the set of two $CeBr_3$ detectors was studied while varying the CF delay from 0.5 ns to 10 ns. During this measurement, the bias voltage of the PMT was set at −1700 V. It has been observed that the best time resolution is obtained with 0.8 ns CF delay, as shown in Fig. 9. The time resolution was also measured by varying the bias voltage of the PMT from −700 V to −1700 V by fixing the CF delay at ~0.8 ns and the results are shown in Fig. 10 for two different cascades of 622–512 keV and 1173–1332 keV. It is concluded from the above measurements, that the detectors can be operated at −1200 V bias voltage of the PMT and with a 0.8 ns CF Delay for obtaining the best time resolution. The best TAC spectra obtained with a ^{60}Co and a ^{106}Ru sources are shown in Fig. 11 in which the FWHM corresponds to the time resolution obtained with two $CeBr_3$ detectors. This gives rise to the time resolution of a single $CeBr_3$ detector at ^{60}Ni and ^{106}Pd energies to be 109(1) ps and 144(1) ps respectively. The time resolution for an $1'' \times 1''$ $CeBr_3$ coupled to a R9779 fast PMT, obtained earlier [11] at ^{60}Ni energies and ^{22}Na annihilation

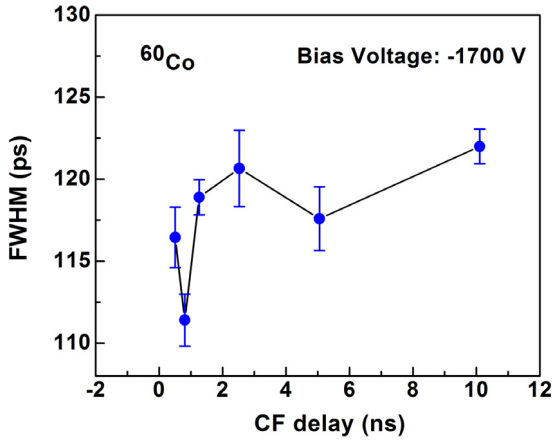

Fig. 9. (Colour online) The time resolution is shown as a function of CF decay.

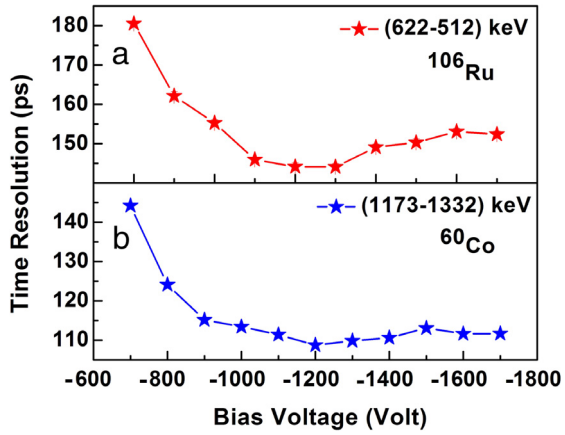

Fig. 10. (Colour online) The time resolution is shown as a function of bias voltage of the PMT.

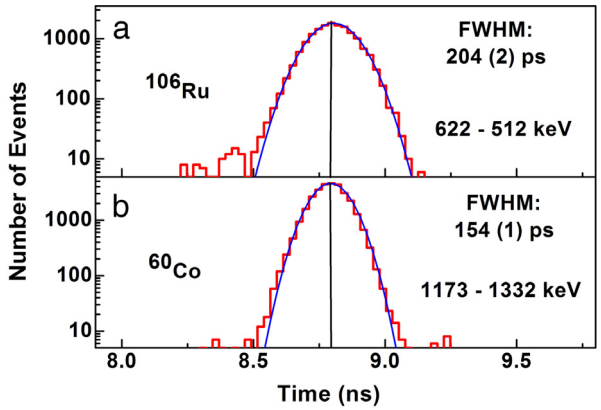

Fig. 11. (Colour online) The TAC spectra obtained with two $CeBr_3$ detectors while using the ^{60}Co and ^{106}Ru source. The obtained FWHM values are indicated in the corresponding plot.

γ energies, are ~120 ps and ~164 ps respectively. An improvement of time resolution by ~10 ps in the present work compared to ref [11] could be attributed to the difference in measurement techniques followed in the two works. In ref [11], time resolution has been measured with a combination of BaF_2-$CeBr_3$ detectors compared to the $CeBr_3$- $CeBr_3$ detectors used in the present case.

4. Fast timing measurement with $CeBr_3$ detectors

If the lifetimes of the excited energy levels are smaller than the time resolution of the fast detector setup then the centroid difference technique has been used until very recently [4,34,35] for the measurement of lifetime ~ few tens of ps for excited nuclear levels. However, the main problem associated with this conventional technique is the energy dependence of the prompt response curve. Also the timing asymmetry present in the branch detectors forces the prompt time calibration for each branch detectors. The GCD [6] and the MSCD [5] methods are proposed very recently that could overcome the above issues involved in fast timing measurement with conventional centroid difference technique and has been possible due to the availability of the detectors like $LaBr_3$(Ce). These methods are based on the distinction between the start and the stop signals of the fast-timing setup in order to unambiguously generate the independent delayed and anti-delayed time spectra. The measurement of the centroid difference between these two time spectra results in a linearly combined mirror-symmetric $\gamma-\gamma$ time-walk characteristics which can be determined precisely, as described in Section 4.2.

The delayed time distribution, experimentally obtained with a set up of two detectors, can be determined from the convolution of the Prompt Response Function (PRF) of the set up with an exponential decay as given by the following equation.

$$D(t) = n\lambda \int_{-\infty}^{t} P(t' - t_0) e^{-\lambda(t'-t_0)} dt' \tag{1}$$

where $P(t' - t_0)$ is the PRF having centroid at t_0 which may be a symmetric Gaussian. n is the number of counts in the time difference spectrum and $\lambda = \frac{1}{\tau}$ is the transition probability related to the mean life time τ of the nuclear level associated with the $\gamma-\gamma$ cascade. The centroid of the distribution can be determined experimentally by the following equation.

$$C_{expt} = \langle t \rangle = \frac{\int_{t_{min}}^{t_{max}} tn(t)dt}{\int_{t_{min}}^{t_{max}} n(t)dt} \tag{2}$$

where $n(t)$ is the number of counts in channel t and related to $D(t)$, the time distribution defined in Eq. (1). The statistical error in the determination of the centroid can be obtained from the variance of $D(t)$. Eqs. (1) and (2) are valid for the ideal case, where no background of any kind contributes. If only random background contributes (not time-correlated, constant time background), Eq. (1) only needs to be extended by a constant. For Eq. (2), the integration limits t_{min} and t_{max} have to be chosen appropriately; they should be set just at the beginning and the end of the time peak. This is in order to avoid possibly large systematic errors related to the random background sporadically distributed on the left and the right of the time peak. The centroid of a delayed time spectrum (C^D) is shifted from the centroid of the PRF (C^P) by the mean lifetime τ and thus the following equations can be written for a particular γ ray cascade having energies E_{feeder} and E_{decay} [27].

$$\tau = C^D(E_{feeder}, E_{decay}) - C^P(E_{feeder}, E_{decay}) \tag{3}$$

$$= C^P(E_{decay}, E_{feeder}) - C^{AD}(E_{decay}, E_{feeder}). \tag{4}$$

C^D and C^{AD} are the centroids for the delayed and anti-delayed time spectrum respectively. These two time spectra are obtained for the same $\gamma-\gamma$ cascade and the position of their centroid depends on whether the feeding (decay) transition is detected with the start (stop) detector or otherwise. Using the known $\gamma-\gamma$ cascades with known mean lifetimes τ and by experimentally determining the centroids C^D

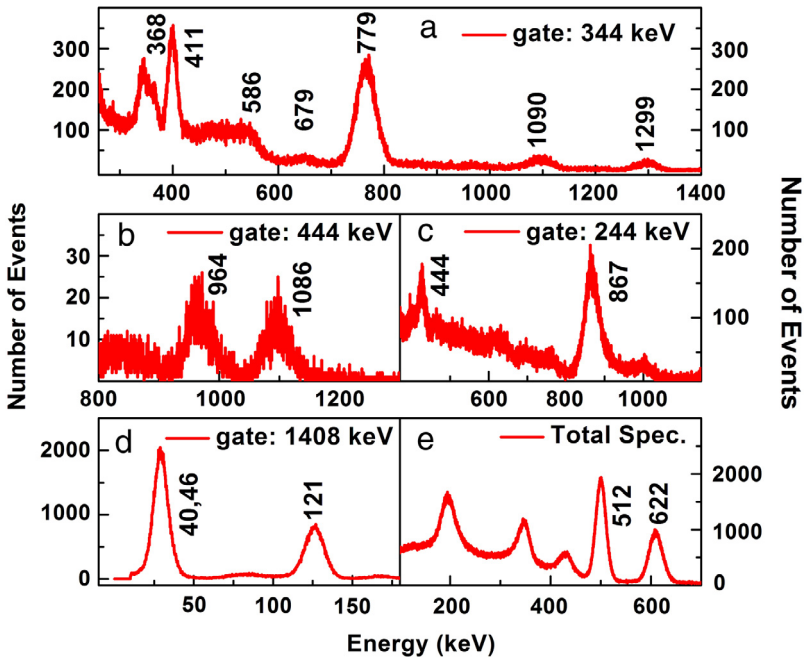

Fig. 12. (Colour online) The energy spectra obtained by gating on different reference energies, viz. (a) 344 keV, (b) 444 keV, (c) 244 keV and (d) 1408 keV transitions, by using the ^{152}Eu source. (e) The energy spectrum obtained with ^{106}Ru source is shown.

and/or C^{AD}, the prompt response functions can be calibrated. However, as the time response from the two detectors for a particular Full Energy Peak (FEP) are inherently different by nature, the calibration procedure becomes difficult and is prone to many systematic errors. The introduction of GCD (MSCD) method overcomes this problem. The following subsections describe the methodologies and results obtained for the lifetime measurements with several $CeBr_3$ detectors using the GCD (MSCD) methods.

4.1. MSCD and GCD techniques

The GCD technique [6,27] is applicable for a timing setup with N numbers of fast timing detectors, where the delayed and anti-delayed time distributions are derived from the superposition of $\frac{N(N-1)}{2}$ time difference spectra obtained from all possible combination of the timing setup. The MSCD method is a special case of GCD with $N = 2$.

The centroid difference (ΔC), representing the time shift between the delayed and anti-delayed time distributions, is given by the following equation [27].

$$\begin{aligned}&\Delta C(E_{feeder}, E_{decay}) = \\ &C^{D}(E_{feeder}, E_{decay}) \\ &-C^{AD}(E_{decay}, E_{feeder}) \\ &= 2\tau + PRD(E_{feeder}, E_{decay})\end{aligned} \tag{5}$$

where

$$PRD(E_{feeder}, E_{decay}) = C^{P}(E_{feeder}, E_{decay}) - C^{P}(E_{decay}, E_{feeder}).$$

The above Eq. (5) is valid with the assumption that the time distributions are generated from the time response of the FEPs and there is no background contribution. However, the experimental $\Delta C(E_{feeder}, E_{decay})$ (ΔC_{Exp}) for any $\gamma - \gamma$ cascade is determined by setting energy gates on the two energies E_{feeder} and E_{decay} and thus includes background contributions in addition to the FEP. Hence, a correction related to the underlying background is required. This can be done by using the following equation.

$$\Delta C_{FEP} = \Delta C_{Exp} + \frac{\Delta C_{Exp} - \Delta C_{Comp}}{\pi} \tag{6}$$

where π is the peak to background (ptb) ratio and ΔC_{Comp} (time response of the background) is to be considered for the background underlying both the photopeaks [5,8]. For the GCD technique, an average centroid difference ($\overline{\Delta C}$) is obtained from the N detector setup with an appropriate background correction and that can be used to determine the average PRD ($\overline{PRD}$).

The calibration of PRDs can be done as a function of energy by considering,

$$PRD(E_{feeder}, E_{decay}) = PRD(E_{feeder}) - PRD(E_{decay})$$

and

$$PRD(E_{decay}, E_{decay}) = PRD_{decay}(E_{decay}) = 0$$

The above equation represents that PRD = 0, when the 'reference' energy is E_{decay}. This means that the PRD curve crosses the energy axis at the reference energy in the PRD(E_γ) representation. The shape of the PRD curve mainly depends on the PMT gain variance, the CFD shaping delay time and the adjustment of the CFD base line [27] and can be fitted with the following function [36].

$$PRD(E_\gamma) = \frac{a}{\sqrt{E_\gamma + b}} + cE_\gamma + d \tag{7}$$

where a, b, c, d are the constant parameters which are obtained by least square fitting of the data points.

In the present work, the GCD (MSCD) method has been explored for the first time using $CeBr_3$ detectors, to measure lifetimes ~ few ps to few tens of ps. The ^{152}Eu source has been used to generate the PRD curve by using the known level lifetime of the 344 keV level of the ^{152}Gd and the 244, 444 & 1408 keV levels of ^{152}Sm. The known level lifetimes for different cascades from the ^{106}Ru and ^{133}Ba sources were measured and have been described in the following subsection (cf. Sections 4.2 and 4.3).

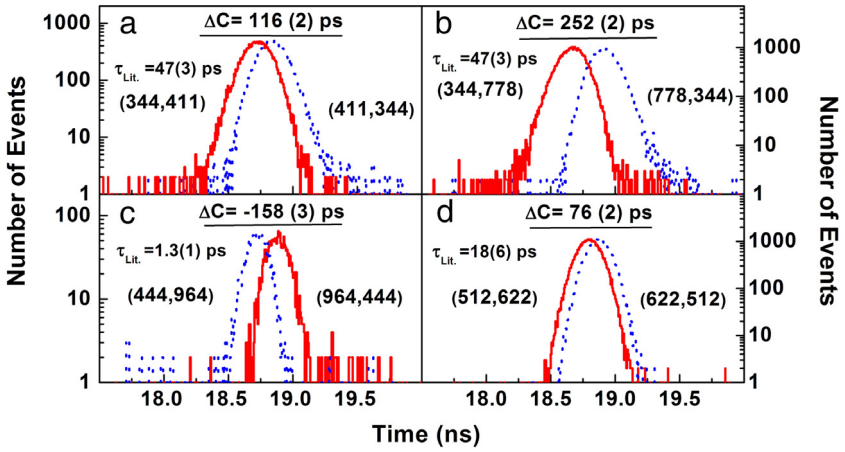

Fig. 13. Few delayed and anti-delayed time spectra obtained with the two $CeBr_3$ detector setup using cascades of ^{152}Gd(a,b), ^{152}Sm(c) and ^{106}Pd(d). The delayed time distributions are shown with blue (dotted) and the anti-delayed with red (solid) line. (For interpretation of the references to colour in this figure legend, the reader is referred to the web version of this article.)

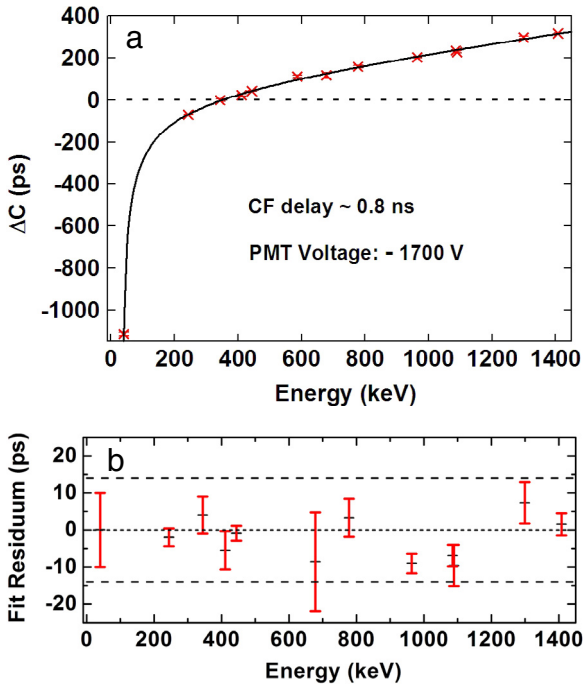

Fig. 14. (Colour online) (a) The PRD curve obtained with two $CeBr_3$ detectors. The solid line shows the fit to these data points by using the function described in Eq. (7). (b) The fit residuum is shown for the data points with respect to a 3σ deviation for the PRD curve.

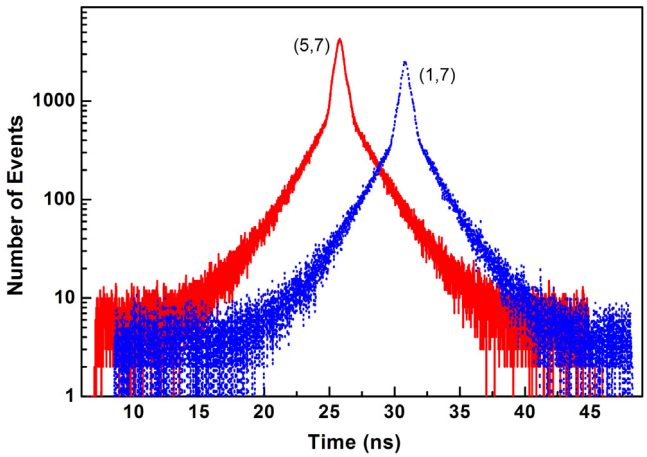

Fig. 15. (Colour online) The time difference spectra obtained with different combinations of $CeBr_3$ detectors of the VENTURE array.

4.2. Results with two $CeBr_3$ detectors

In this measurement, the PRD curve was generated as described above and the PRD calibration was done by following the procedures given in Ref. [27,36]. The relevant gated spectra are shown in Fig. 12, obtained form ^{152}Eu source as well as ^{106}Ru source. The latter has been used to measure the lifetime of the 512 keV level in ^{106}Pd, as described below. During this measurement, the CF delay was set at 0.8 ns and the PMT bias voltage was set at −1700 V. The delayed and anti-delayed time spectra obtained for few of the associated cascades are shown in Fig. 13. The data points for the PRD curve were generated by following the MSCD technique, as described above, and are shown in Fig. 14(a). The error value corresponding to each data point was determined by considering the statistical error for the determination of the centroid as well as the errors in the lifetime values with the associated $\gamma-\gamma$ cascades.

The data points have been fitted to generate the PRD calibration function using Eq. (7). The error in the PRD curve was estimated by calculating the standard deviation (σ) of the experimental data points from the fitted PRD curve and the fit residuum for the data points are shown in Fig. 14(b) with respect to 3σ value (14 ps). Following the generation of calibration curve, the Centroid difference for the 622–512 keV cascade of ^{106}Pd has been determined and shown in Fig. 13d. Using this centroid difference and the PRD values at 512 and 622 keV γ energies, the level lifetime of the 511.9 keV level of ^{106}Pd was measured to be 19(10) ps which closely matches with the literature value [37]. The error in the measured lifetime has been estimated by using both the errors in the centroid difference and the PRD.

4.3. Results with the VENTURE array

In order to generate the $\overline{PRD}$ curve with the VENTURE array, the GCD technique was used in combination with common start timing technique while operating the detectors at −1700 V bias and using a CF delay of 5 ns. The data were gathered with ^{152}Eu, ^{133}Ba and ^{106}Ru sources. During offline analysis, the list mode data were sorted event by event where a valid event was considered only when the ADCs corresponding to the energy of the two detectors (E_i and E_j) and the corresponding TACs (TAC_i and TAC_j) have valid data, decided by the thresholds. For all these events TAC_i and TAC_j were subtracted to

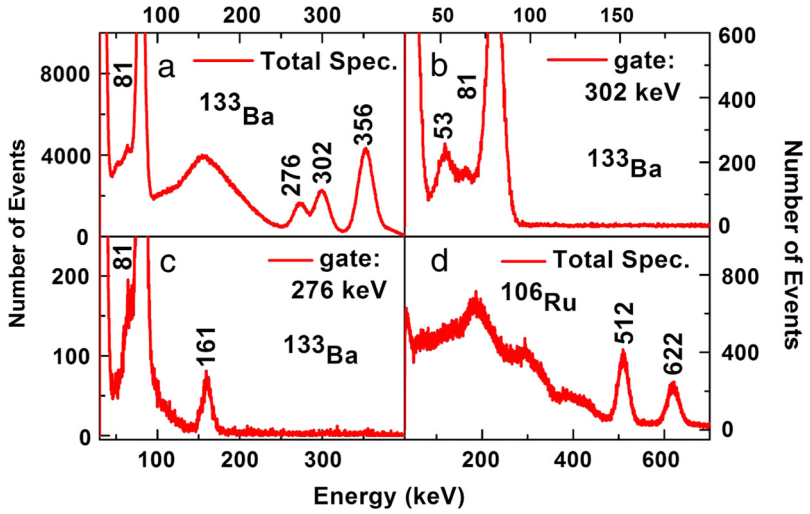

Fig. 16. (Colour online) (a) The total spectrum obtained from ^{133}Ba source. The 302 keV gate, (b) 276 keV gate (c) and total spectrum from ^{106}Ru source (d) have been shown.

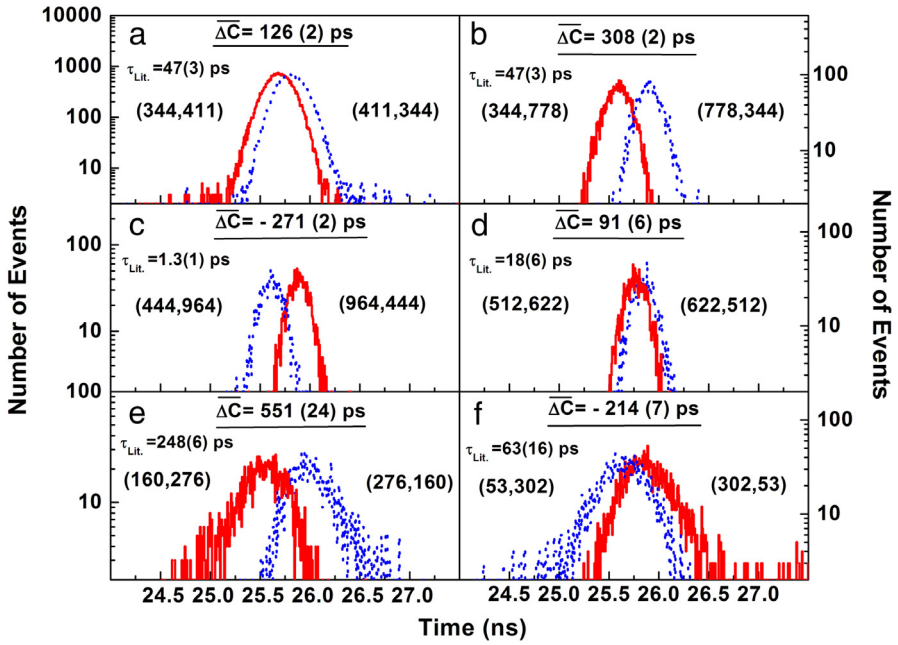

Fig. 17. The delayed and anti-delayed time spectra obtained with the cascades of ^{152}Eu, ^{106}Ru and ^{133}Ba sources using VENTURE array. The delayed time distributions are shown with blue (dotted) and the anti-delayed with red (solid) line. (For interpretation of the references to colour in this figure legend, the reader is referred to the web version of this article.)

generate the time difference spectra, TAC$_{ij}$ ($i > j$), between any two detectors of the array, as shown in Fig. 15. These time distribution spectra are equivalent to the ones reported in Ref. [27] and thus confirms that the electronics used in the present work has the ability to be used with GCD technique. Twenty eight combinations were thus generated which were time calibrated before generating the total TDS by adding these individual TAC$_{ij}$s. While doing so, the gain matched energy of the detector i and detector j from each event were kept in two energy parameters. These two energy parameters and the total TDS represented the VENTURE array as equivalent to a two detector set up. The energy gates were put in these two final energy parameters to project the total TDS in order to generate the delayed and anti-delayed time spectra followed by the generation of the $\overline{PRD}$ curve of the array. The FWHM values have been determined from the time distribution curves obtained for the VENTURE array for several cascades as shown in Table 1. The FWHM values show a maximum degradation ~ 25% compared to the ones obtained with two detector measurement and this was observed to be mainly contributed by the worst combination of the detectors present in the array.

Table 1
FWHM values obtained for different energy cascades with the VENTURE array.

Cascade	FWHM (ps)	
(keV)	2-det.	VENTURE
344–778	227(1)	276(4)
444–964	190(4)	235(5)
512–622	204(2)	250(5)
1173–1332	154(8)	188(3)

The centroid differences were measured for different cascades in ^{152}Sm, ^{152}Gd, ^{106}Pd and ^{133}Cs nuclei. Some representative energy spectra are shown in Fig. 16 and the representative delayed and anti-delayed time spectra are given in Fig. 17. While generating the delayed and anti-delayed time spectra for PRD determination, those combinations were not considered which displayed false coincidence

Table 2
The measurement of level lifetime for different levels of ^{106}Pd and ^{133}Cs, using VENTURE array.

Nucleus	Level	Cascade (keV)	$\overline{\Delta C}$	$\overline{PRD}$	τ (ps)	
					pres. work	Lit.
^{106}Pd	511.9 keV 2^+	622–512	91(6)	58(14)	17(8)	18(6) [37]
^{133}Cs	160.6 keV $\frac{5}{2}^+$	276–161	551(24)	103(14)	224(14)	248(6) [31]
^{133}Cs	383.8 keV $\frac{3}{2}^+$	53–302	−214(7)	−342(14)	64(8)	63(16) [31]

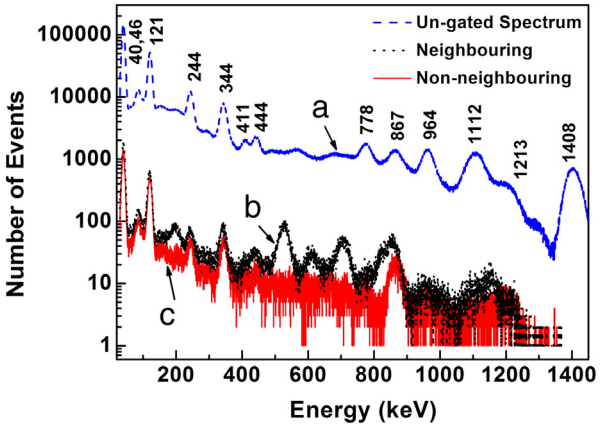

Fig. 18. (Colour online) (a) The ungated energy spectrum. (b) The 244 keV gated spectrum using neighbouring detectors showing 'ghost peak' (c) The 244 keV gated spectrum using non-neighbouring detectors which show clean peaks.

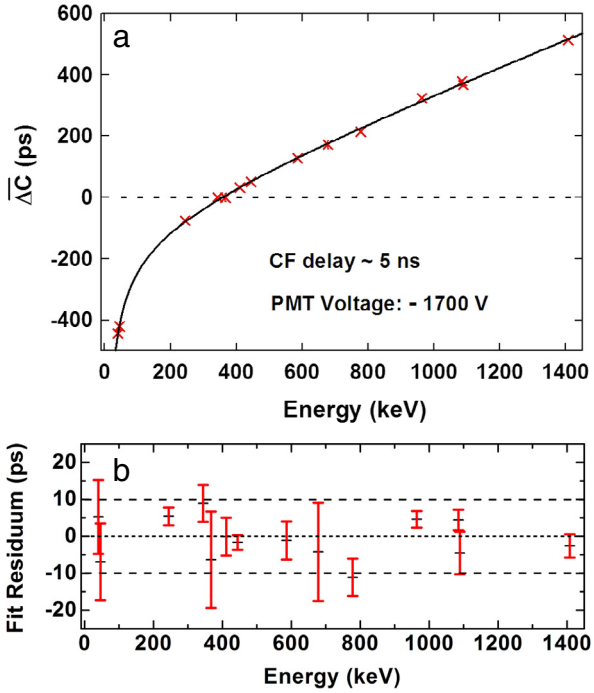

Fig. 19. (Colour online) (a) The $\overline{PRD}$ curve obtained with the VENTURE array is shown. The solid line shows the fit to the data points by using the function described in Eq. (7). (b) The fit residuum is shown for the data points with respect to a 3σ deviation for the PRD curve.

due to back-scattered γ rays coming from the Compton scattered events at some other neighbouring detectors. This was understood from the appearance of 'ghost peaks' in 244 kev gated spectrum shown in Fig. 18, which is similar to the observation with an array of $LaBr_3$ detectors [8]. The $\overline{PRD}$ curve, generated from the centroid differences obtained with the ^{152}Eu source and by fitting the data points with Eq. (7) is shown in Fig. 19(a). The Fit residuum has been displayed in Fig. 19(b) by showing the data points with respect to the 3σ standard deviation (~10 ps), obtained as the error in PRD determination. The obtained standard deviation (σ) ~3 ps shows the possibility of the measurement of nuclear level lifetime down to few ps. Table 2 shows the centroid differences obtained for the 511.9 keV level in ^{106}Pd, and the 160.6 & 383.8 keV levels in ^{133}Cs, obtained from the decay of ^{106}Ru and ^{133}Ba sources respectively. The level lifetimes obtained for these levels by using the above $\overline{PRD}$ calibration function have also been displayed in the table. The background correction was made, as described in Eq. (6), whenever required. The errors in the final lifetime value has been calculated by considering all possible errors present in the measurement which are the standard error in $\overline{PRD}$ and also the error in the centroid shifts calculated with required background correction. All the lifetimes could be reproduced in the present measurement with the VENTURE array. The level lifetime obtained for the 160.6 keV level of ^{133}Cs show a small deviation from the literature value when measured following the GCD method. The lifetime of this level was also determined by using slope and convolution techniques which resulted in the lifetime values of 247(37) ps and 232(10) ps respectively. The lifetime value obtained for the 160.6 keV level by using the GCD method is similar to the one obtained in earlier works with $LaBr_3$ detectors [36]. The observed deviation might be due to low statistics gathered for the relevant cascade and the related error in the centroid determination.

5. Angular correlation measurement with $CeBr_3$ detectors

The Perturbed Angular Correlation (PAC) measurements have long been used for the measurement of nuclear quadrupole moments and in these works the detectors like BaF_2 [38], HPGe [39] and $LaBr_3$(Ce) [40] have been used, depending on the lifetime of nuclear levels. The $CeBr_3$ detectors can also be a good alternative for performing a very precise PAC study. In the present work, a precise unperturbed angular correlation measurement has been performed placing the detectors on an angular correlation table (c.f. Fig. 3), as discussed in Section 2. The angular correlation was performed by varying the angular position of the detector 3 starting from 90° to 180° at an interval of 10°. The anisotropy histogram at each angle ($W(\theta)$) was obtained with a ^{60}Co source and Fig. 20(a) shows the angular correlation plot for the 1173–1332 keV cascade. The data points were fitted with the known angular correlation function,

$$W(\theta) = 1 + A_2 P_2(Cos\theta) + A_4 P_4(Cos\theta). \quad (8)$$

The experimental A_2 and A_4 values, when compared with the calculated ones (1.02 and 0.009 for A_2 and A_4 respectively) using the F_k coefficients [41], suggest the required solid angle correction factors in A_2 and A_4 to be 1.07 and 0.81 respectively.

The angular correlation measurement was also performed for the 228–49 keV cascade in ^{132}I which was produced from the decay of ^{132}Te(~3d). The Te isotopes were obtained as one of the fission fragments produced from the ^{238}U(α,f) reaction by using α beam from K = 130 cyclotron at VECC, Kolkata. The Te isotopes were separated from the other fission products by radio-chemical separation method

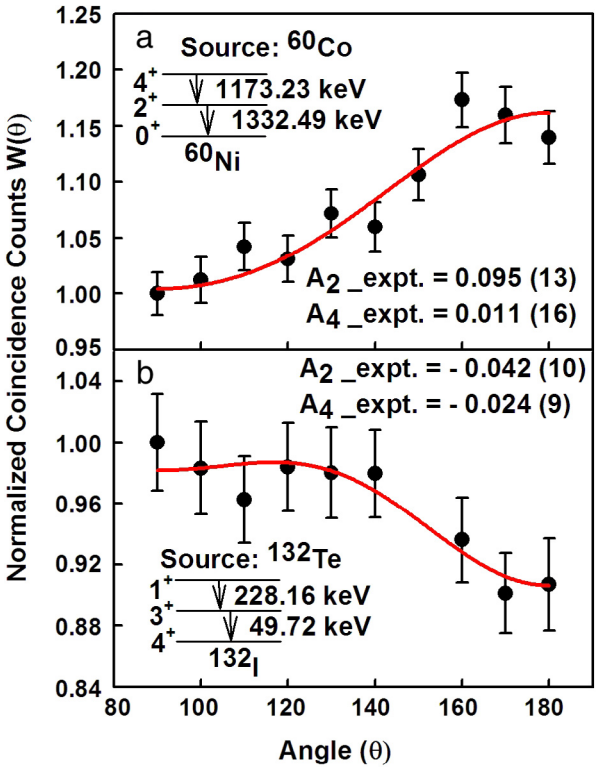

Fig. 20. (Colour online) (a) The angular correlation plot obtained with the 1173–1332 keV cascade from ^{60}Co source. (b) The same obtained for the 228–49 keV cascade from the ^{132}I nucleus.

and thus it was a challenge to gather sufficient statistics required for the angular correlation measurement. The angular correlation result has been displayed in Fig. 20(b) and the A_2 and A_4 coefficients were obtained from the least square fitting of the data points using Eq. (8) followed by the solid angle corrections. The A_2 value is found to be close to the theoretical one, calculated by considering the multipolarity of these transitions as obtained from the Ref. [42].

6. Summary

A fast timing array (VENTURE), consisting of multiple $CeBr_3$ detectors, has been developed for the measurement of lifetimes down to few ps. The array has been utilised to measure the lifetime of several nuclear levels, viz., 511.9 keV level of ^{106}Pd and 383.8, 160.6 keV levels of ^{133}Cs nuclei. The present work demonstrates, for the first time, the use of $CeBr_3$ detectors in the lifetime measurement of nuclear level using GCD (MSCD) technique. The application of common start timing technique has also been implemented with GCD method for the first time in the present work. The prompt time resolution of the array was found to be degraded by ~25%, compared to the two detector measurement, which was contributed mainly by the worst detector pair of $CeBr_3$ detectors used in the array. In the present measurement, the PRD calibration for the VENTURE array could be obtained with an accuracy of less than 10 ps (3σ standard deviation) or ~3ps (1σ standard deviation). The present work, thus, displays the capability of the VENTURE array for precise measurements of nuclear level lifetimes down to few picoseconds. This work also presents the use of $CeBr_3$ detectors in the $\gamma-\gamma$ angular correlation measurement. The angular correlation coefficients have been measured for the 1173–1332 keV cascade in ^{60}Co and 228–49 keV cascade in ^{132}I. In the process of developing the present array, the $CeBr_3$ detector of dimension 1″ dia ×1″ thick and coupled to a Hamamatsu R9779 PMT has been characterised for its spectroscopic properties like energy response, energy resolution, absolute efficiency and time resolution. The operational condition for the detectors at the bias voltage of −1200 V and a CF delay of 0.8 ns were found to be optimum on the basis of linear response and best time resolution of the detectors. The present work reports a time resolution of 144(1) ps and 109(1) ps respectively for the ^{106}Ru and ^{60}Co photopeaks and an energy resolution of 4.5% at 622 keV.

Acknowledgements

The authors acknowledge the support of BRNS for developing the VENTURE array through the PRF project (Sanction No. 2013/38/02-BRNS/1927 for PRF, BRNS, dated 16 October 2013). The support of the staffs of the K = 130 cyclotron at VECC kolkata for delivering good quality beam is acknowledged. The mechanical engineering group, VECC, is sincerely acknowledged for the fabrication of the angular correlation table used in the present work. Dr. Paul Schotanus of M/s Scionix is gratefully acknowledged for providing a buffer preamplifier for the testing with the supplied detectors. Mr. R. K. Chatterjee is acknowledged for preparing good quality Uranium targets. VECC workshop is acknowledged for the design and fabrication of the support structures of the $CeBr_3$ detectors and the liquid sample holder used in the present work. Dr. A. Chatterjee, MSU, Baroda, is sincerely acknowledged for his help regarding the use of LAMPS software in the data analysis. Dr. P. K. Pujari, Head, RCD, BARC is gratefully acknowledged for his constant support in the progress of the work through BRNS funding.

References

[1] P. Petkov, A. Dewald, P. von Brentano, Nucl. Instrum. Methods Phys. Res. A 560 (2006) 564.
[2] A. Dewald, S. Harissopulos, P. von Brentano, Z. Phys. A 334 (1989) 163.
[3] A.Z. Schwarzschild, E.K. Warburton, Annu. Rev. Nucl. Sci. 18 (1968) 265.
[4] H. Mach, R.L. Gill, M. Moszyski, Nucl. Instrum. Methods Phys. Res. A 280 (1989) 49.
[5] J.M. Régis, et al., Nucl. Instrum. Methods Phys. Res. A 622 (2010) 83.
[6] J.M. Régis, et al., Nucl. Instrum. Methods Phys. Res. A 726 (2013) 191.
[7] M. Rudigier, et al., Phys. Rev. C 91 (2015) 044301.
[8] J.M. Régis, et al., Nucl. Instrum. Methods Phys. Res. A 763 (2014) 210.
[9] T. Bhattacharjee, et al., Phys. Rev. C 88 (2013) 014313.
[10] R. Billnert, et al., Nucl. Instrum. Methods Phys. Res. A 647 (2011) 94.
[11] L.M. Fraile, et al., Nucl. Instrum. Methods Phys. Res. A 701 (2013) 235.
[12] N. D'Olympia, et al., Nucl. Instrum. Methods Phys. Res. A 728 (2013) 31.
[13] G. Lutter, et al., Nucl. Instrum. Methods Phys. Res. A 703 (2013) 158.
[14] P. Gauss, et al., Nucl. Instrum. Methods Phys. Res. A 608 (2008) 297.
[15] U. Ackermann, et al., Nucl. Instrum. Methods Phys. Res. A 786 (2015) 5.
[16] Paul Lecoq, Alexander Gektin, Mikhail Korzhik, Inorganic Scintillators for Detector Systems, Springer, 2017 (Chapter 5).
[17] F.G.A. Quarati, et al., Nucl. Instrum. Methods Phys. Res. A 729 (2013) 596.
[18] F.G.A. Quarati, et al., Nucl. Instrum. Methods Phys. Res. A 735 (2014) 655.
[19] F.G.A. Quarati, et al., Nucl. Instrum. Methods Phys. Res. A 629 (2011) 157.
[20] P. Dorenbos, J.T.M. de Haas, C.W.E. van Eijk, IEEE Trans. Nucl. Sci. 51 (3) (2004) 1289.
[21] Soumik et al. Bhattacharya, Proc. DAE-BRNS Symp. Nucl. Phys. 61 (2016) 98.
[22] R. Raut, et al., Proc. DAE-BRNS Symp. Nucl. Phys. 47B (2004) 578.
[23] S.S. Alam, et al., Proc. DAE-BRNS Symp. Nucl. Phys. 61 (2016) 316.
[24] S.S. Alam, et al., Proc. DAE-BRNS Symp. Nucl. Phys. 61 (2016) 318.
[25] http://www.tifr.res.in/~pell.
[26] N. Mărginean, et al., Eur. Phys. J. A 46 (2010) 329.
[27] J.M. Régis, et al., Nucl. Instrum. Methods Phys. Res. A 823 (2016) 72.
[28] R. Brun, et al., GEANT3, CERN - DD/EE/84-1, 1986.
[29] J.M. Régis, et al., Nucl. Instrum. Methods Phys. Res. A 811 (2016) 42.
[30] M.J. Martin, Nucl. Data Sheets 114 (2013) 1497.
[31] Yu. Khazov, A. Rodionov, F.G. Kondev, Nucl. Data Sheets 112 (2011) 855.
[32] E. Browne, J.K. Tuli, Nucl. Data Sheets 114 (2013) 1849.
[33] G. Duchene, et al., Nucl. Instrum. Methods Phys. Res. A 432 (1999) 90.
[34] H. Mach, et al., Nuclear Phys. A 523 (1991) 197.
[35] Z. Bay, Phys. Rev. 77 (1949) 419.
[36] J.M. Régis, et al., Nucl. Instrum. Methods Phys. Res. A 684 (2012) 36.
[37] D. De Frenne, A. Negret, Nucl. Data Sheets 109 (2008) 943.
[38] Satyendra K. Das, Sanjay V. Thakare, Tilman Butz, J. Phys. Chem. Solids 70 (2009) 778.
[39] D.L. Balabanski, et al., Phys. Rev C 83 (2011) 014304.
[40] D. Banerjee, et al., Hyperfine Interact. 198 (1–3) (2011) 193.
[41] H. Morinaga, T. Yamazaki, In - Beam Gamma-Ray Spectroscopy, North-Holland Publishing Company, New York, 1976.
[42] Yu Khazov, A.A. Rodionov, S. Sakharov, Balraj Singh, Nucl. Data Sheets 104 (2005) 497.